Supplementary Information: dissolvable fluidic time delays for programming multi-step assays in instrument-free paper diagnostics

Barry Lutz, Tinny Liang, Elain Fu, Sujatha Ramachandran, Peter Kauffman, Paul Yager

Section 1: Parameters contributing to time delay in sugar-treated strips

Purpose: identify the relative contributions of parameters affecting capillary pressure and fluidic resistance in sugar-based time delays

System: strips with dried sugar wet out by saturated sugar solution

We performed an experiment similar to that of **Figure 2** but using saturated sugar solution as the wicking fluid. This system suppresses dissolution of the dried sugar, thus the pore structure of the strips should remain constant during wet-out, and the framework of the conventional Lucas-Washburn relationship should apply (as it does for untreated strips, so long as the meaning of r is not over-interpreted). Strips were prepared by applying different sugar concentrations and drying, followed by wicking saturated sugar solution containing dye into the strips (**Figure S1A**). **Figure S1B** shows strips after 2.2 hours. Surprisingly, the wicking rate was comparable for all strips despite a wide range of applied sugar concentrations (0-70% of saturation).

Case 1: buffer solution wicking into untreated nitrocellulose (no sugar)

$$W = 9.15 \ mm^2/s$$

Case 2: saturated sugar solution wicking into sugar-treated strips

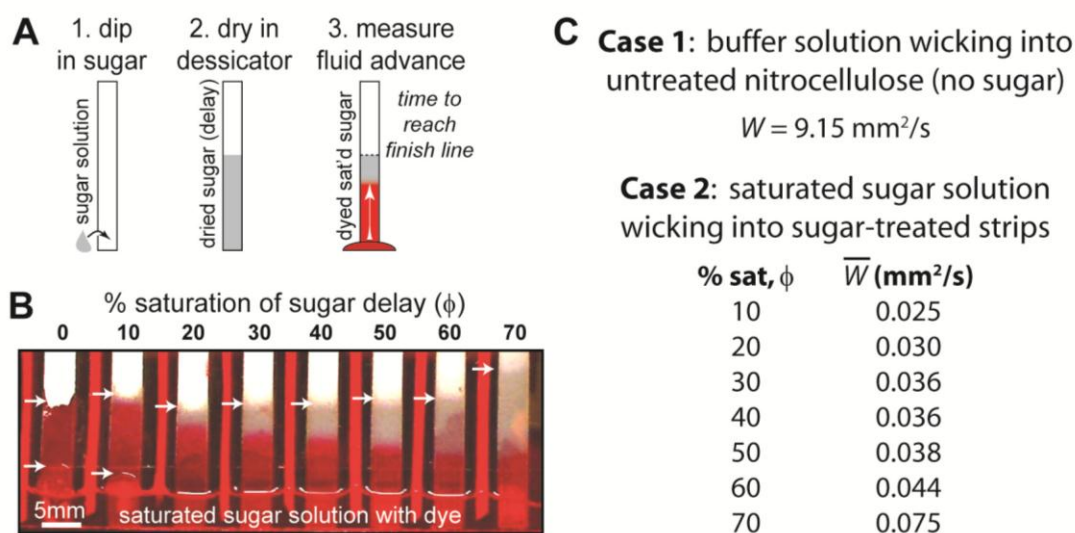| % sat, ϕ	$\overline{W}$ (mm²/s)
10	0.025
20	0.030
30	0.036
40	0.036
50	0.038
60	0.044
70	0.075

Figure S1. Wicking of saturated sugar solution into sugar-treated strips. A) Sugar solutions of different concentrations were applied to strips and dried, and saturated sugar solution containing dye was wicked into the strips. B) Image of the experiment at 2.2 hours. Arrows indicate the location of the fluid front. Also visible is a separation of dye that is increasingly apparent with increasing concentration of applied sugar; this can be explained by a chromatographic effect due to partitioning of the dye into the dried sugar due to the equilibrium dissolution and deposition between the saturated sugar fluid (initially dyed) and the dried sugar solid (no dye initially). The extent of wicking is comparable in all strips. In the 0% and 10% strips, the fluid source rose above the base fluid level due to capillary action between the strip and the front wall of the container; the wicking length was measured from the top of the fluid source (lower white arrows). C) Washburn coefficients (W) calculated from experiments for Case 1 and Case 2 as denoted in the main article; all sugar-treated strips gave W of comparable magnitude.

The Washburn coefficient (**W**) for buffer wicking into untreated nitrocellulose (**Case 1**) was calculated from the first strip in **Figure 2** (calculated from arrival time at a given length).

$$L^2 = \frac{\gamma \cdot \cos\theta \cdot r}{4\eta} \cdot t = W \cdot t \quad W = 9.15\,mm^2/s$$

The Washburn coefficients for saturated sugar wicking into sugar-treated strips (**Case 2**) were calculated from the experiment in **Figure S2** (calculated from arrival time at a given length).

$$\overline{L}^2 = \frac{\overline{\gamma} \cdot \cos\overline{\theta} \cdot \overline{r}}{4\overline{\eta}} \cdot \overline{t} = \overline{W} \cdot \overline{t} \quad \overline{W} = 0.025 - 0.075\,mm^2/s$$

For strips treated with 0% sugar to 70% sugar, **W** ranged from 0.025 mm^2/s to 0.075 mm^2/s (**Figure S1C**). The small trend may be meaningful or may be due to experimental bias, but the important point is that the magnitude of change is far too small to account for the observed range of time delays. The relative contributions from terms can be estimated by taking the ratio of the two Lucas-Washburn expressions for fluid front arrival at a given length (**L**).

$$
\underbrace{\frac{\overline{t}}{t}}_{} = \underbrace{\frac{W}{\overline{W}}}_{\substack{\text{measured in strips:} \\ \sim 120-360}} = \underbrace{\frac{\gamma}{\overline{\gamma}} \cdot \frac{\cos\theta \cdot r}{\cos\overline{\theta} \cdot \overline{r}}}_{\text{calculated here: } \sim 1} \cdot \underbrace{\frac{4\overline{\eta}}{4\eta} \approx \frac{\overline{\eta}}{\eta}}_{\substack{\text{fluid property:} \\ \sim 200}}
$$

The observed ratio of arrival times (~120-360) is explained almost entirely by the contribution of the viscosity ratio (~200). Thus, the term containing contributions from surface tension, contact angle, and pore size is of order one; we discuss each component of this term:

- **γ** ratio: it is expected to be near one since all fluids contain surfactant above the critical micelle concentration; this is expected to dominate the surface tension and hold it relatively constant.
- **cos θ** ratio: it is reasonable that this term is near one, since all fluids contain surfactant, and sugar is a wettable material.
- **r** ratio: the Lucas-Washburn expression was derived for a single cylindrical pore, and the 1st order radius term has embedded in it three contributions: 1) the wetted perimeter (affects capillary force, $2\pi r$), 2) the void volume (affects the volume of fluid required to achieve a given length of penetration, πr^2), and 3) the fluidic resistance (which has a very strong dependence, $1/r^4$). These three contributions are mathematically connected for a single pore (via the pore radius) and reduce to a 1st order dependence (**r**). In complex porous media, the relationship between **L** and **t** ($L^2 \sim t$) often holds very well, but the radius term cannot be interpreted literally. Specifically, in our case the material has 1) non-uniform pore size distribution, 2) intersecting pores, and 3) unknown modification of pore size and distribution by the dried sugar. For our experiments, the **r** term appears to have a weak dependence similar to that for the single pore case.

Conclusion: in sugar delays, the combined contributions from surface tension, contact angle, and pore size are small, and the contribution from viscosity accounts almost entirely for the observed time delays.

Section 2. Simple model of sugar distribution for complete dissolution

Purpose: derive a simplified model to estimate the fraction of wetted length occupied by a saturated fluid front under complete dissolution and without viscous fingering

System: strips with dried sugar wet out by buffer

Figure S2 illustrates the assumptions used to derive the fraction of the fluid front assuming that all sugar is dissolved by the advancing front up to the point of fluid saturation. A single pore model is also shown to illustrate the concept, but no assumptions are made about the pore structure.
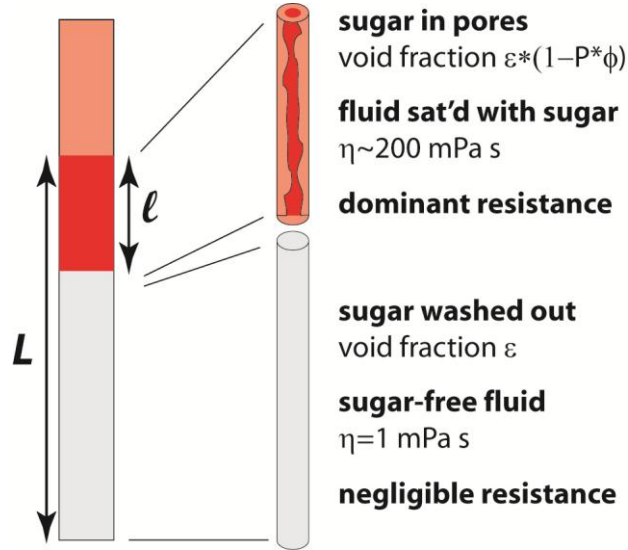

sugar in pores
void fraction $\varepsilon*(1-P*\phi)$

fluid sat'd with sugar
$\eta \sim 200$ mPa s

dominant resistance

sugar washed out
void fraction ε

sugar-free fluid
$\eta = 1$ mPa s

negligible resistance

*Figure S2. Illustration of a simple model to estimate the fraction of the wetted region (**L**) occupied by a saturated sugar region (**ℓ**) when all dried sugar is dissolved by the leading front up to the point of saturation. The leading region has a viscosity of saturated sugar ($\eta \approx 200$ mPa·s) and smaller pores relative to the washed out region, thus the relative fluidic resistances are expected to scale roughly as **ℓ***200/**L***1 and the resistance will be dominated by the sugar-rich leading edge under the conditions tested.*

The length of the wetted region (**L**) includes a leading saturated sugar region (**ℓ**) that is expected to scale with the amount of sugar dried onto the strip (ϕ is the % saturation of the sugar solution applied to the strip before drying). The ratio **ℓ**/**L** can be calculated from a mass balance between the mass of sugar dissolved from the region of the strip **L-ℓ** and the mass of sugar contained in the saturated fluid region **ℓ**.

mass of sugar dissolved from the region **L-ℓ**   mass of sugar in the saturated fluid region **ℓ**

$$W \cdot H \cdot (L - \ell) \cdot \varepsilon \cdot C_{sat} \cdot \varphi = W \cdot H \cdot \ell \cdot \varepsilon \cdot (1 - P \cdot \varphi) \cdot C_{sat}$$

volume of sugar-containing fluid   concentration   volume of fluid of sugar-coated pores (void   concentration of
applied to the strip before drying   of applied sugar   volume) in the region ls   sat'd sugar fluid

W and **H** are the width and thickness of the nitrocellulose strips, respectively, ε is the void fraction of the untreated nitrocellulose, C_{sat} is the concentration of sucrose saturated in water at room temperature, ϕ is the percent saturation of the sugar fluid applied to the strip before drying, and **P** is the ratio of dry solid sugar volume to the fluid volume of saturated sugar from which it was created (**P**=0.56 cm^3 solid/cm^3 soln based on: dry sucrose density 1.578 g solid/cm^3 solid; weight % and density of a sucrose solution saturated at 20°C of 0.667 g sugar/g soln and 1.329 g soln/cm^3 soln, respectively) [material properties from: Z. Bubník, P. Kadlec, D.

Urban and M. Bruhns, *Sugar technologists manual: Chemical and physical data for sugar manufacturers and users*, Dr. Albert Bartens Verlag, Berlin, Germany, 1995]. A simple expression results from canceling terms.

$$\frac{l_s}{L} = \frac{\varphi}{1 + \varphi \cdot (1 - P)}$$

To a first approximation, fraction of wetted strip length containing saturated fluid (ℓ /L) scales with the concentration of applied sugar (ϕ); the term in the denominator (ϕ*(1-P)) has a modest effect. The fraction of strip length containing saturated sugar fluid (ℓ /L) is constant throughout the wetting process, and scales approximately with the sugar loading, ℓ /$L \approx \phi$.

Conclusion: assuming complete dissolution of the dried sugar by an intact advancing fluid front, the fraction of the wetted region (**L**) occupied by saturated sugar (**ℓ**) scales approximately with the sugar loading, ℓ /**L** $\approx \phi$.

Section 3. Simple model of relative resistances for complete dissolution

Purpose: derive a simplified model for the relative fluidic resistances of the saturated sugar region and the washed out region for complete dissolution without viscous fingering (intact viscous front)

System: strips with dried sugar wet out by buffer

If the fluid front remained intact (as represented in **Figure S2**), the fluidic resistances of the two regions – saturated sugar and washed out (sugar-free) fluid – would represent series resistances that are additive (and as noted above, have a constant relative magnitude throughout the wet-out process). Considering viscosity effects alone, the resistances of the saturated sugar region and washed out (sugar-free) region, respectively, scale as

$$\ell \cdot \overline{\eta} \quad \text{and} \quad L \cdot \eta$$

Using the approximation $\ell /L \approx \phi$ for convenience, the relative contribution of resistances is

$$\frac{R(\text{sat'd sugar region})}{R(\text{washed out region})} \approx \frac{\ell \cdot \overline{\eta}}{L \cdot \eta} \approx \frac{L \cdot \varphi \cdot \overline{\eta}}{L \cdot \eta} = \varphi \cdot \frac{\overline{\eta}}{\eta} = 200 \cdot \varphi$$

Thus, the net resistance would be expected to be dominated by the saturated sugar leading region for all conditions tested here (ϕ>0.1 gives a resistance ratio >20). Pore occlusion effects that were not included in this estimate would further reinforce this assertion.

We expect a similar scaling to apply to the time delays for sugar-treated strips. For the largest sugar loading tested (ϕ=0.7), the relative arrival time would be roughly 200*0.7=140, which is of comparable magnitude to the delay found in **Figure 2** (relative arrival time ~80). However, the simplified model suggests that the relative arrival times would scale linearly with sugar loading (ϕ), while the delays observed in **Figure 2** are very non-linear. Thus the simplified model for an intact viscous front greatly overpredicts the time delays for most of the tested conditions. As described in the text, the intact front assumed in this model was actually disrupted by viscous fingering, which would be expected to reduce time delays compared to this prediction. For small sugar loading, the viscous front was rapidly disrupted by viscous fingering, while viscous fingers took longer to form at high sugar loading. This could explain the strong non-linear behavior observed. Verification of this greatly simplified model would require extensive experiments not yet performed, but the analysis shows that viscous effects are sufficient in magnitude to explain the observed time delays and the reduction in time delays compared to this prediction is consistent with viscous fingering.

Conclusions: assuming complete dissolution of the dried sugar by an intact advancing fluid front, 1) the fluidic resistance is expected to be dominated by the sugar-rich leading front for all conditions tested here, 2) this simple model predicts larger time delays than observed and a linear dependence on sugar loading compared to the highly non-linear dependence observed, and 3) disruption of the sugar-rich leading front by viscous fingering is consistent with the observed reduction in time delays and the non-linear dependence on sugar loading.

Section 4: Comparison of arrival times in simple strips and paper networks

The selection of delay times in paper networks is complicated by at least two factors: 1) paper network delays are wetted from two sides, while simple strips (**Figure 2**) are wetted from one side, and 2) the wicking force provided by the network is different from simple strips and changes over time. **Figure S3** shows delay times measured from the paper network of **Figure 4** compared to those for simple strips of **Figure 2**. Data for simple

strips was estimated by interpolation between data points in two cases (54% and 65%), so quantitative comparison is not appropriate. However, the results show that delay times from the paper network were approximately comparable to those for simple strips, and perhaps somewhat longer.
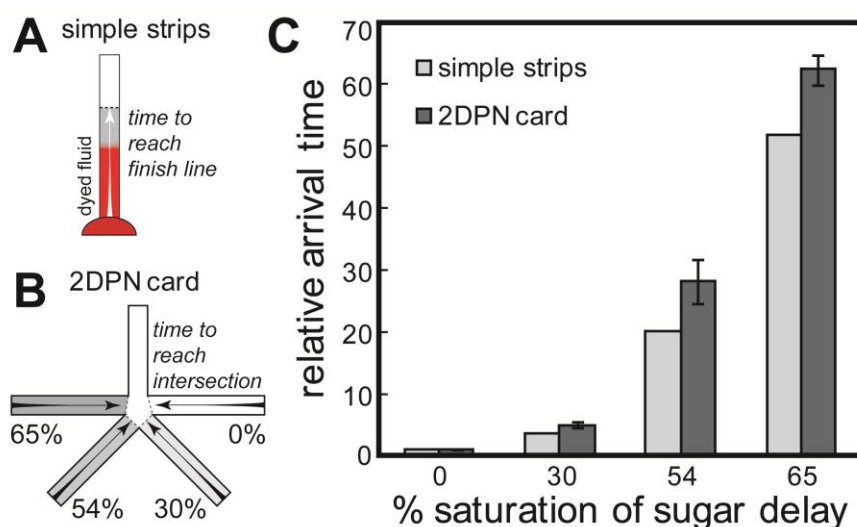

Figure S3. *Comparison of time delays in simple strips and a 2DPN. A) For the simple strips of* **Figure 2**, *arrival times were estimated from the data for the same sugar concentrations used in the paper network. B) For the 2DPN of* **Figure 4**, *the arrival time of each fluid at the intersection was measured from videos. C) For both cases, the arrival times are shown as a ratio of sugar-treated strips (or leg) to the untreated strip (or leg). The two cases showed comparable delay times; delays in paper networks appear somewhat longer, but this is not conclusive since delays were estimated for 54% and 65% sugar in simple strips (and error bars were not reported for interpolated values).*

Section 5: Some factors in delay selection for paper networks

Figure S4A qualitatively illustrates the goals for selection of time delays in paper networks. Time delays should be sufficiently long to prevent fluid from a leg from entering the main channel before delivery of fluid from the prior leg has ceased. Also, an additional delay should be designed between each leg to account for error in timing contributed by each delay.

Figure S4B illustrates this concept for the assay device shown in **Figure 5**. The amount of fluid in each pad was estimated at each time point from the video. As a pad was drained, the loss of fluid was visualized as a retreating fluid front in the pad (drained regions of the pad were lighter than fluid-filled regions, see Video). As a course measure of the drainage time course, a darkness threshold was applied to identify filled and unfilled regions at each time point, and the percent filled was estimated. We note that this is a course estimate but is sufficient to illustrate the drainage period for each pad.

Figure S4B shows the approximate time periods for delivery of each fluid into the main leg. Some fluid from each pad was required to fill the delay region (roughly the gray area, verified from videos as the time point at which fluid began to exit each leg into the main channel). Fluid 1 was depleted before delivery of fluid 2 began. Similarly, a clean time gap was seen between delivery steps for fluids 2 and 3. In contrast, fluid 3 continued to "leak" slowly near the end of delivery, and fluids 3 and 4 flowed simultaneously for a short period (although the flowrate of fluid 3 was relatively small). This slow delivery was likely due to the difficulty of drawing fluid from the furthest extents of the glass fiber pad (those farthest from the nitrocellulose strip; note that only one edge of the glass fiber pad overlapped the strip. In retrospect, allowing the glass fiber pad to overlap completely with the nitrocellulose strip would have been a more robust arrangement). In any case, **Figure S4**

shows that delivery was largely successful, with time separation between delivery from three legs, and an undesirable (but small) overlap in delivery for the last two legs.

Approximate delivery rates were calculated from the slope of drainage plot during the delivery period. The first fluid (red) was delivered quickly, as expected for initial wet-out under Washburn-Lucas flow (i.e., the flow is initially fast due to the short path length, and slows over time). Subsequent fluids were delivered at slower rates, as expected, since the strip was fully wet. Delivery rate decreased by small amounts for each subsequent leg, which could be due to filling of the cellulose waste pad, slower flow through broken barriers of higher sugar concentration, or a combination of the two. In any case, the decrease in delivery rate was modest.

The data of **Figure 5** did not include replicates, so we do not have the data needed to evaluate the errors in the immunoassay. Error is accommodated by "dormant period" between each fluid delivery during which fluid does not flow, but the total volumes of each fluid delivered are the same (controlled by the amount of fluid on each pad). The step most likely to be affected by error is the application of gold amplification reagents, since non-flowing reagent may continue to amplify the signal. Since signal in **Figure 5** increases linearly with time, we would expect immunoassay errors to be comparable to flow timing errors. Delivery time errors were 9-19% (n=5) in the paper network (see **Figure 4**), with the largest deviation occurring in the first step (one that does not involve a delay).
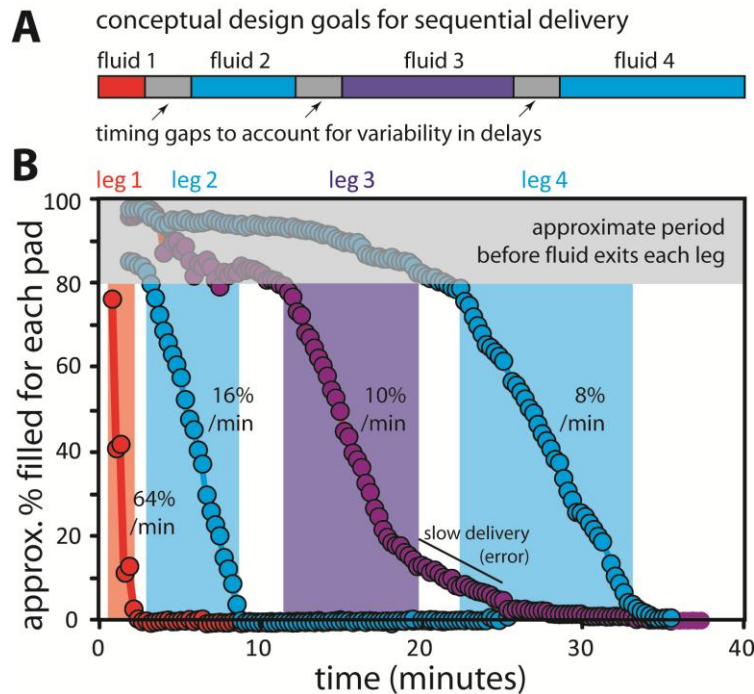

Figure S4. *Illustration of issues affecting selection of delay times in network devices. A) Conceptual illustration of the design goal. Delay times should be chosen to prevent simultaneous flow of fluids from different legs. Additional delay time should be included to account for errors in the delay time for each leg. B) Characterization of drainage from each pad as a function of time. The percentage filled was estimated from video images during operation of the assay device from **Figure 5**. The gray area at top represents the approximate volume of fluid required to fill the delay region before fluid delivery begins. The shaded regions below indicate the approximate time periods during which each fluid was delivered. Delivery rates were estimated from the slope of data during the delivery periods.*